Communications in Applied and Industrial Mathematics,
ISSN 2038-0909, **1**, 1, (2010) 237–257
DOI: 10.1685/2010CAIM475

Modular algorithms for the numerical solution of the flow rate boundary value problem in fluid-dynamics

Christian Vergara[1]

[1] *Dipartimento di Ingegneria dell'Informazione e Metodi Matematici*
Università degli Studi di Bergamo, Italy
christian.vergara@unibg.it

Communicated by Alessandro Iafrati

Abstract

In many engineering fluid dynamics problems, the prescription of defective boundary conditions, such as the flow rate, on artificial boundaries can be source of numerical inaccuracies. At the practical level, in the engineering literature this problem has been solved by choosing a velocity profile fitting the given defective datum (*practical approach*). After a brief description of this method and of its limitations, we review two strategies based on the introduction of Lagrange multipliers. In particular we focus on the derivation and the analysis of the continuous formulations and on the algebraic properties of the related linear systems. We describe two algorithms for their solution which are modular, that is could be solved by using pre-existing fluid solvers. Finally, we present some realistic numerical results showing the effectiveness of the strategies considered in comparison with the practical approach.

Keywords: `Navier-Stokes equations, Flow rate condition, Lagrange multipliers.`

AMS Subject Classification: `65M12, 65M60, 76D05`

1. Introduction.

The mathematical modelization of many fluid-dynamics phenomena leads to Partial Differential Problems, like the *Navier-Stokes* or the *Euler* equations. In view of the solution of these problems, it is very important to specify a suitable domain in which the equations are solved. In many engineering fluid dynamics problems, this computational domain is part of a system or a network. In this case, a part of the boundary does not correspond to a physical wall, and it is just introduced to limit the domain of interest. The prescription of boundary conditions on such *artificial* boundaries can be source of numerical inaccuracies. In particular, in different contexts of internal fluid-dynamics there is sometimes the need of managing numerically *defective boundary data sets*, namely data that are

Received 2010 01 14, in final form 2010 06 12
Published 2010 06 21

not enough to have a mathematically well posed problem.

A fluid dynamic field in which it is usually necessary to manage with defective boundary problems is *haemodynamics* (see [2,3,13]). In fact, it is quite typical in this case to have only average data from the clinical measurements. For instance, it can be happen in solving fluid problems in a network of pipes to have at the inlet only the flow rate (*flow rate problem*). In this context, the problem of the defective boundary data has been analyzed at the mathematical and numerical levels since about ten years (see [4,12]).

In this work, we describe the *Augmented formulation* introduced in [3,13] for the numerical treatment of the flow rate problem. In particular, we review two algorithms for its numerical solution, which are *modular*, that is which can be solved by using pre-existing fluid-dynamics classical codes. The aim of this work is to highlight the differences of the solutions obtained by using these schemes and the classical *practical approach* in a realistic numerical simulation obtained in the human carotid.

The outline of the work is as follows. In Section 2.1 we introduce the Navier-Stokes equations for incompressible, Newtonian fluids. In Section 2.2 we define the flow rate boundary value problem, whilst in Section 2.3 we describe the practical approach commonly used in the engineering community. In Section 3 we introduce the Augmented formulation, whilst in Section 4 we present two modular numerical strategies for its solution. Finally, in Section 5 we present some numerical results coming from biomedical applications.

2. Navier-Stokes equations, flow rate and boundary conditions

2.1. *General settings*

Referring to the computational domain $\Omega \subset \mathbb{R}^d$, $d = 2, 3$, in Figure 1, let us consider the *Navier-Stokes equations* for a homogeneous incompressible Newtonian fluid (see [5,9]):

$$(1) \qquad \begin{cases} \rho \dfrac{\partial \boldsymbol{u}}{\partial t} - \mu \triangle \boldsymbol{u} + \rho(\boldsymbol{u} \cdot \nabla)\boldsymbol{u} + \nabla p = \rho \boldsymbol{f}, \quad (t, \boldsymbol{x}) \in Y_T \\ \nabla \cdot \boldsymbol{u} = 0, \quad (t, \boldsymbol{x}) \in Y_T \\ \boldsymbol{u}|_{t=0} = \boldsymbol{u}_0, \quad \boldsymbol{x} \in \Omega \end{cases}$$

where $\boldsymbol{u}(t, \boldsymbol{x})$ is the velocity field, μ is the dynamic viscosity (assumed to be constant), $p(t, \boldsymbol{x})$ the pressure, ρ the constant density, T the final time, $\boldsymbol{u}_0(\boldsymbol{x})$ the *initial condition* and $\boldsymbol{f}(t, \boldsymbol{x})$ a forcing term. When we neglect the convective term $\rho(\boldsymbol{u} \cdot \nabla)\boldsymbol{u}$, we recover the so called *Stokes equations*. Otherwise, when the convective term is replaced by $\rho(\boldsymbol{\beta} \cdot \nabla)\boldsymbol{u}$, with $\boldsymbol{\beta}$ a given velocity field, we have the *Oseen equations*.

DOI: 10.1685/2010CAIM475

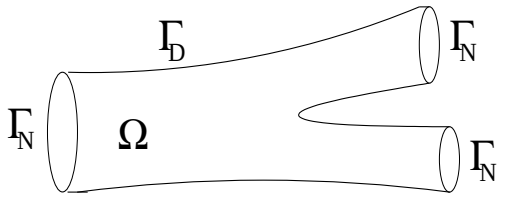

Fig. 1. Reference computational domain Ω.

From the mathematical viewpoint, the 3D (2D) fluid-dynamics problem, described by the incompressible Navier-Stokes equations, requires the assignment of three (two) scalar conditions on each boundary point. Namely, referring to Figure 1, we can prescribe the velocity field (*Dirichlet* boundary condition):

$$\boldsymbol{u}|_{\Gamma_D} = \boldsymbol{g}, \quad t \in (0,T], \tag{2}$$

or the *stress tensor* (*Neumann*/natural boundary condition):

$$(-p\boldsymbol{n} + \mu \nabla \boldsymbol{u}\ \boldsymbol{n})|_{\Gamma_N} = \boldsymbol{h}, \quad t \in (0,T], \tag{3}$$

where $\boldsymbol{g}(t,\boldsymbol{x}) \in \boldsymbol{H}^{1/2}(\Gamma_D)$ and $\boldsymbol{h}(t,\boldsymbol{x}) \in \boldsymbol{H}^{-1/2}(\Gamma_N)$ are given boundary functions and $\boldsymbol{n}(\boldsymbol{x})$ is the unit normal vector to $\partial\Omega$.

In view of the numerical discretization of equations (1), (2) and (3), we introduce a suitable *variational formulation* (see [9]). Let us set:

$$(\boldsymbol{v},\boldsymbol{w}) = \int_\Omega \boldsymbol{v}\cdot\boldsymbol{w}\, d\omega, \qquad b(q,\boldsymbol{v}) = -\int_\Omega q\, \nabla\cdot\boldsymbol{v}\, d\omega$$

and the following space

$$\boldsymbol{V} = \boldsymbol{H}^1_{\Gamma_D}(\Omega) = \{\boldsymbol{v} \in \boldsymbol{H}^1(\Omega) :\ \boldsymbol{v}|_{\Gamma_D} = \boldsymbol{0}\},$$

$\boldsymbol{H}^1(\Omega)$ being the usual Sobolev space. Moreover, given a generic Hilbert space $\boldsymbol{W}$, let us denote

$$\boldsymbol{W}^* = \{\boldsymbol{v} \in \boldsymbol{W} :\ \nabla\cdot\boldsymbol{v} = 0\}.$$

We obtain the following (see [9]):

Problem 1. *Given* $\boldsymbol{u}_0 \in \boldsymbol{L}^2(\Omega)^*$, $\boldsymbol{f} \in L^2(0,T;\boldsymbol{L}^2(\Omega))$, *find* $\boldsymbol{u} \in L^2(0,T;\boldsymbol{V}) \cap L^\infty(0,T;\boldsymbol{L}^2(\Omega))$ *and* $p \in L^2(0,T;L^2(\Omega))$, *such that, for each* $t \in (0,T]$*:*

$$\begin{cases} \rho\Big(\dfrac{\partial \boldsymbol{u}}{\partial t}, \boldsymbol{v}\Big) + a(\boldsymbol{u},\boldsymbol{v}) + \rho((\boldsymbol{u}\cdot\nabla)\boldsymbol{u},\boldsymbol{v}) + b(p,\boldsymbol{v}) = \rho(\boldsymbol{f},\boldsymbol{v}) + (\boldsymbol{h},\boldsymbol{v})_{L^2(\Gamma_N)} \\ b(q,\boldsymbol{u}) = 0 \end{cases}$$

for all $\boldsymbol{v} \in \boldsymbol{V}$ *and* $q \in L^2(\Omega)$ *and with the initial condition* $\boldsymbol{u}|_{t=0} = \boldsymbol{u}_0$.

In Problem 1, we have set $a(\boldsymbol{v},\boldsymbol{w}) = \mu \int_\Omega \nabla\boldsymbol{v} : \nabla\boldsymbol{w}\, d\omega$.

2.2. *Flow rate boundary conditions*

In many fluid-dynamics problems the numerical simulations aim at obtaining some quantitative informations on a local phenomenon, confined in a domain that is part of a complex system or a network. Therefore, in order to obtain numerical results with a reasonable computational cost, it is necessary to consider a bounded domain including the zone of interest. In this computational domain a subset of the boundary corresponds to a real/physical wall. For example, in the domain in Figure 2 (right), Γ_w is a physical boundary. For what concernes this portion of boundary, we assume the hypothesis of *no-slip* condition, i.e. the complete adherence of the fluid on the wall. This hypothesis, if the motion occurs in rigid domains, leads to the homogeneous Dirichlet boundary condition:

$$\boldsymbol{u}|_{\Gamma_w} = \mathbf{0}, \quad t \in (0, T]$$

On the other hand, another part of the boundary ($\Gamma_0 \cup \Gamma_1 \cup \Gamma_2$ in Figure 2,

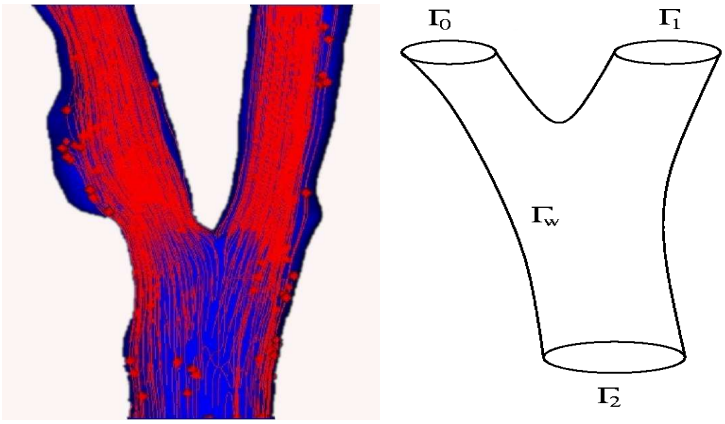

Fig. 2. An example of a truncated domain Ω: a tipical vascular district. We detect the "physical" boundary (the vascular wall Γ_w) and the "artificial" boundaries Γ_0, Γ_1 and Γ_2 (courtesy of A. Veneziani).

right) does not correspond to a physical boundary but it is just introduced to limit the domain of interest. The surfaces belonging to this part of the boundary are called *artificial* sections, since they are the interface of the district with the other parts of the circulatory system. For example, this situation occurs often in haemodynamics, where the computational domain is a truncated part of the complex vascular tree. In Figure 3 an example of such domain in haemodynamics is shown.

As already pointed out in the Introduction, the prescription of suitable boundary conditions on the artificial sections is a major issue in many

DOI: 10.1685/2010CAIM475

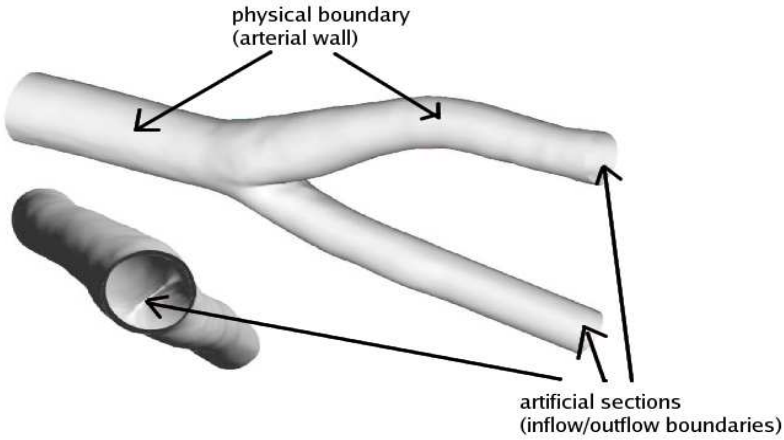

Fig. 3. Carotid bifurcation geometry: it is possible to detect the "physical" and the "artificial" boundaries (cast by D. Liepsch - FH Munich)

fluid-dynamics problems. Sometimes it is just difficult to obtain realistic informations on such boundaries and furthermore, when available, they are often referred to an average datum. Namely, let us suppose to have $m+1$ artificial section Γ_i, $i = 0, \ldots, m$. For example, if we refer to the computational domain Ω in Figure 2, right, we have $m = 2$. It is worth considering *flow rate* conditions on such surfaces

$$\rho \int_{\Gamma_i} \boldsymbol{u} \cdot \boldsymbol{n} \, d\gamma = Q_i, \quad \forall i = 0, \ldots, m, \quad t \in (0, T] \tag{4}$$

where $Q_i = Q_i(t)$ are given. Since we refer to a rigid domain Ω, let us notice that we can prescribe arbitrarily the flow rates (4) on all but one the artificial sections, for example on $\Gamma_1, \Gamma_2, \ldots, \Gamma_m$. Indeed, due to the mass conservation and the rigidity of the walls, on Γ_0 we have:

$$Q_0 = \rho \int_{\Gamma_0} \boldsymbol{u} \cdot \boldsymbol{n} \, d\gamma = -\sum_{i=1}^{m} \rho \int_{\Gamma_i} \boldsymbol{u} \cdot \boldsymbol{n} \, d\gamma = -\sum_{i=1}^{m} Q_i. \tag{5}$$

Moreover, for the sake of simplicity, let us suppose here and in the sequel of this work that $\rho = 1$. Conditions (4) are clearly not sufficient to achieve a well-posed mathematical problem that needs pointwise conditions like (2) or (3). Specific strategies in order to fill this gap are therefore mandatory.

2.3. *State of the art of the flow rate problem: A practical approach*

The most common strategy used in the engineering literature in order to complete these defective boundary data consists in choosing *a priori* a velocity profile $\boldsymbol{g}_i$ on each section Γ_i where the flux is prescribed, fitting the given flow rate Q_i. Therefore, we make use of a Dirichlet boundary conditions like (2), such that (see Figure 4):

$$\int_{\Gamma_i} \boldsymbol{g}_i \cdot \boldsymbol{n}\, d\gamma = Q_i, \quad \forall i = 0, \ldots, m, \quad t \in (0, T],$$

with the values Q_i satisfying the constraint (5). This approach is not al-

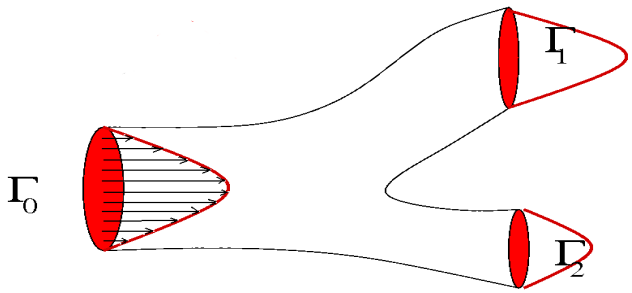

Fig. 4. Example of a selected velocity profile prescribed at the artificial sections.

ways feasible, for istance for real geometries when an analytical expression for the profile is not available. In particular let us notice that an analytical solution is available only for a cylindrical domain perfused by a steady or a sinusoidal flow rate. In these cases we refer to the *Poiseuille* and the *Womersley* solution, respectively (see [17]). For a different flow rate perfusing a cylinder, a feasible approach is to decompose the wave form of the flow rate into its Fourier components and to combine basic Womersley solutions correspondly to each frequency component. Strictly speaking, this approach is exact only if the problem at hand is linear. Therefore, when the Navier-Stokes equations are considered and, in particular, for increasing values of the *Reynolds number* $Re = \rho V L/\mu$, with V and L a characteristic velocity and a characteristic length respectively, this approach gives an approximate "feasible" solution. In general, for a realistic computational domain it is not possible to know *a priori* the exact velocity profile to be prescribed on the boundaries neither in the steady nor in the periodic case. Nevertheless, in these cases, if the artificial sections are circular, it is a common practice to impose anyway a parabolic, a Womersley or a flat velocity profile. Since the

DOI: 10.1685/2010CAIM475

numerical solution is strongly affected by the arbitrary selected profile, the computational domain is quite often enlarged letting the profile to develop, in order to reduce the effect of the profile prescription in the zone of interest. Obviously, this approach presents the drawback of increasing the computational costs. In particular, the higher is the Reynolds number the larger has to be the extra zone as the fluid needs more space to develop fully. In particular, for steady flows in a cylindrical domain, it is possible to define a characteristic length equal approximately to $0.058 \cdot D \cdot Re$ (where D is the diameter of the inlet section) at which a centreline velocity is within 1% of its final value (see [16]). A similar dependence on Re is recognized also for a non cylindrical domain and for unsteady flows. However, in the unsteady case the development of the profile can be problematic. For example, it has been shown in [10] that for high Reynolds numbers, in a cylindric domain perfused by a periodic flux, the enlargement of 40 diameters may not be sufficient to recover the analytical (Womersley) solution if a parabolic profile is prescribed as boundary condition at the inlet. If the section where the flow rate is prescribed is not circular, some authors proposed to use anyway the Womersley solution as boundary condition, extending the computational domain by some arterial diameters, such that the cross-section transition leads to a perfectly circular artificial section in the actual geometry. Finally, we highlight that in some realistic cases, a wrong choice of the prescribed velocity profile, could lead to an error also in the computation of global quantities, such as the flow division (see e.g. [7]). Although quite simple and popular, this approach can be therefore source of serious inaccuracies, beside leading to an increased computational effort.

3. Augmented formulation of the flow rate problem

Let us consider the domain $\Omega \subset \mathbb{R}^d$, $d = 2, 3$, represented in Figure 5 and the following unsteady Oseen problem:

$$\begin{cases} \dfrac{\partial \boldsymbol{u}}{\partial t} - \mu \triangle \boldsymbol{u} + (\boldsymbol{\beta} \cdot \nabla)\boldsymbol{u} + \nabla p = \boldsymbol{f}, \quad (t, \boldsymbol{x}) \in Y_T \\ \nabla \cdot \boldsymbol{u} = 0, \quad (t, \boldsymbol{x}) \in Y_T \\ \boldsymbol{u}|_{t=0} = \boldsymbol{u}_0(\boldsymbol{x}), \quad \boldsymbol{x} \in \Omega \end{cases} \tag{6}$$

together with the boundary conditions:

$$\begin{cases} \boldsymbol{u}|_{\Gamma_w} = \boldsymbol{0}, \quad t \in (0, T] \\ (p\boldsymbol{n} - \mu \nabla \boldsymbol{u}\ \boldsymbol{n})|_{\Gamma_0} = \boldsymbol{0}, \quad t \in (0, T] \\ \displaystyle\int_{\Gamma_i} \boldsymbol{u} \cdot \boldsymbol{n}\, d\gamma = Q_i, \quad i = 1, 2, \ldots, m, \quad t \in (0, T]. \end{cases} \tag{7}$$

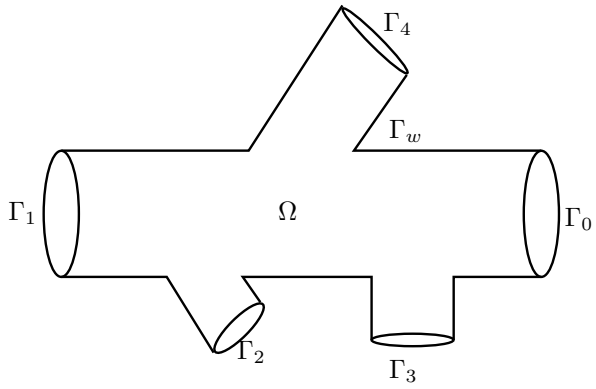

Fig. 5. Domain Ω of interest in the flow rate problem. In this case we have $m = 4$.

It is worth noticing that fluxes are imposed on all the artificial sections apart from Γ_0. Let us consider the following functional:

$$F(\boldsymbol{v}) = \left(\frac{\partial \boldsymbol{v}}{\partial t}, \boldsymbol{v}\right) + \frac{1}{2}a(\boldsymbol{v}, \boldsymbol{v}) + \frac{1}{2}((\boldsymbol{\beta} \cdot \nabla)\boldsymbol{v}, \boldsymbol{v}) - (\boldsymbol{f}, \boldsymbol{v}). \tag{8}$$

By minimizing this functional in the space $\boldsymbol{V}^*$ (where $\Gamma_D \equiv \Gamma_w$), we obtain a variational formulation of problem (6) with the following boundary conditions:

$$\begin{cases} \boldsymbol{u}|_{\Gamma_w} = \boldsymbol{0}, \quad t \in (0, T], \\ (p\boldsymbol{n} - \mu \nabla \boldsymbol{u}\ \boldsymbol{n})|_{\Gamma_0} = \boldsymbol{0}, \quad t \in (0, T], \\ (p\boldsymbol{n} - \mu \nabla \boldsymbol{u}\ \boldsymbol{n})|_{\Gamma_i} = \boldsymbol{0}, \quad i = 1, \ldots, m, \quad t \in (0, T]. \end{cases}$$

This corresponds to a free minimization of the functional (8). On the other hand, if we want to take into account the supplementary information given by the flow rate boundary conditions $(7)_3$, we can think to minimize the previous functional with the constraint given by these conditions. With this aim, let us introduce the following definition:

$$< \phi_i, \boldsymbol{v} > := \int_{\Gamma_i} \boldsymbol{v} \cdot \boldsymbol{n}\, d\gamma, \quad \forall i = 1, \ldots, m,$$

where $\phi_i \in V'$, $i = 1, \ldots, m$ and $< \cdot, \cdot >$ denotes the duality between V' and $\boldsymbol{V}$. With the previous definition we can formulate the flow rate condition in terms of a continous and linear functional. In particular, let us consider the following constrained minimization problem:

Problem 2. *Find* $\boldsymbol{u} \in \boldsymbol{V}^*$ *such that*

$$\begin{cases} \min_{\{\boldsymbol{w} \in \boldsymbol{V}^*\}} F(\boldsymbol{w}) \\ < \phi_j, \boldsymbol{w} >= Q_j, \quad j = 1, \ldots, m. \end{cases}$$

DOI: 10.1685/2010CAIM475

In order to solve this problem we make use of a *Lagrange multipliers* approach, i.e. we minimize the Lagrangian functional obtained by adding to the functional F the constraints $(7)_3$ multiplied by the Lagrange multipliers (see [9]). In this way, the Lagrangian functional associated to Problem 2 becomes:

$$L(\boldsymbol{w}, \xi_1, \dots, \xi_n) = \frac{1}{2}\Big(\frac{\partial \boldsymbol{w}}{\partial t}, \boldsymbol{w}\Big) + \frac{1}{2}a(\boldsymbol{w}, \boldsymbol{w}) + \frac{1}{2}((\boldsymbol{\beta}\cdot\nabla)\boldsymbol{w}, \boldsymbol{w}) +$$

$$-(\boldsymbol{f}, \boldsymbol{w}) + \sum_{j=1}^{m} \xi_j(< \phi_j, \boldsymbol{w} > -Q_j),$$

As usual for constrained minimization problems, we can make use of a saddle point formulation:

Problem 3. *Find* $\boldsymbol{u} \in \boldsymbol{V}^*$ *and* $\lambda_1, \dots, \lambda_n \in \mathbb{R}$ *such that, for each* t*:*

$$L(\boldsymbol{u}, \lambda_1, \dots, \lambda_m) = \min_{\{\boldsymbol{w}\in\boldsymbol{V}^*\}} \max_{\{\xi_1,\dots,\xi_m\in\mathbb{R}\}} \{L(\boldsymbol{w}, \xi_1, \dots, \xi_m)\},$$

where λ_j are the Lagrange multipliers associated to constraints $(7)_3$. Let us consider the function Ψ obtained evaluating L in $(\boldsymbol{u} + \varepsilon\boldsymbol{v}, \lambda_j + \alpha_j\eta_j,\ j = 1, \dots, m)$, with $\boldsymbol{v}$ and η_j the variations (costant in time) from the solution $(\boldsymbol{u}, \lambda_i)$:

$$\Psi(\varepsilon, \alpha_1, \dots, \alpha_m) = L(\boldsymbol{u} + \varepsilon\boldsymbol{v}, \lambda_1 + \alpha_1\eta_1, \dots, \lambda_n + \alpha_n\eta_m).$$

Differentiating with the respect to ε, we obtain:

$$\frac{d\Psi(\varepsilon, \alpha_1, \dots, \alpha_m)}{d\varepsilon} = \Big(\frac{\partial \boldsymbol{u}}{\partial t}, \boldsymbol{v}\Big) + \varepsilon\Big(\frac{\partial \boldsymbol{v}}{\partial t}, \boldsymbol{v}\Big) + a(\boldsymbol{u}, \boldsymbol{v}) + \varepsilon a(\boldsymbol{v}, \boldsymbol{v}) + ((\boldsymbol{\beta}\cdot\nabla)\boldsymbol{u}, \boldsymbol{v}) +$$

$$+\varepsilon((\boldsymbol{\beta}\cdot\nabla)\boldsymbol{v}, \boldsymbol{v}) - (\boldsymbol{f}, \boldsymbol{v}) + \sum_{j=1}^{m} \lambda_j < \phi_j, \boldsymbol{v} > + \sum_{j=1}^{m} \alpha_j\eta_j < \phi_j, \boldsymbol{v} >$$

and with the respect to α_j:

$$\frac{d\Psi(\varepsilon, \alpha_1, \dots, \alpha_m)}{d\alpha_j} = \eta_j(< \phi_j, \boldsymbol{u} > -Q_j) + \eta_j\varepsilon < \phi_j, \boldsymbol{v} > .$$

By forcing

$$\begin{cases} \dfrac{d\Psi(0, 0, \dots, 0)}{d\varepsilon} = 0, \\ \dfrac{d\Psi(0, 0, \dots, 0)}{d\alpha_j} = 0, \quad j = 1, \dots, m, \end{cases}$$

we obtain:

$$\begin{cases} \left(\dfrac{\partial \boldsymbol{u}}{\partial t}, \boldsymbol{v}\right) + a(\boldsymbol{u}, \boldsymbol{v}) + ((\boldsymbol{\beta} \cdot \nabla)\boldsymbol{u}, \boldsymbol{v}) + \displaystyle\sum_{j=1}^{m} \lambda_j < \phi_j, \boldsymbol{v} >= (\boldsymbol{f}, \boldsymbol{v}), \quad \forall \boldsymbol{v} \in \boldsymbol{V}^* \\ \eta_j(< \phi_j, \boldsymbol{u} > - Q_j) = 0, \quad \text{for} \quad j = 1, \ldots, m, \qquad \forall \eta_j \in \mathbb{R}. \end{cases}$$

By proceeding in a similar way, with an explicit treatment of the incompressibility constraint, we obtain the following *augmented* variational formulation for the problem given by (6) and (7):

Problem 4. *Given* $\boldsymbol{u}_0 \in \boldsymbol{V}^*$, $\boldsymbol{f}(t) \in L^2(0,T;\boldsymbol{L}^2(\Omega))$, $\boldsymbol{\beta} \in L^\infty(0,T;\boldsymbol{L}^\infty(\Omega))$ *and* $\boldsymbol{Q}(t) \in (C^0([0,T]))^m$ *(with* $\int_{\Gamma_j} \boldsymbol{u}_0 \cdot \boldsymbol{n}\, d\gamma = Q_j(0)$*), find* $\boldsymbol{u}(t) \in L^2(0,T;\boldsymbol{V}) \cap L^\infty(0,T;\boldsymbol{L}^2(\Omega))$, $p \in L^2(0,T;L^2(\Omega))$ *and* $\boldsymbol{\lambda} \in (L^2(0,T))^m$ *such that*

$$(9) \quad \begin{cases} \left(\dfrac{\partial \boldsymbol{u}}{\partial t}, \boldsymbol{v}\right) + a(\boldsymbol{u}, \boldsymbol{v}) + ((\boldsymbol{\beta} \cdot \nabla)\boldsymbol{u}, \boldsymbol{v}) + b(p, \boldsymbol{v}) + \displaystyle\sum_{j=1}^{m} \lambda_j \int_{\Gamma_j} \boldsymbol{v} \cdot \boldsymbol{n}\, d\gamma = \\ \qquad\qquad = (\boldsymbol{f}, \boldsymbol{v}), \quad (t, \boldsymbol{x}) \in Y_T \\ b(q, \boldsymbol{u}) = 0, \qquad (t, \boldsymbol{x}) \in Y_T, \\ \boldsymbol{u}|_{t=0} = \boldsymbol{u}_0, \qquad \boldsymbol{x} \in \Omega, \\ \displaystyle\int_{\Gamma_i} \boldsymbol{u} \cdot \boldsymbol{n}\, d\gamma = Q_i \quad \forall i = 1, \ldots, m, \qquad t \in (0, T], \end{cases}$$

for all $\boldsymbol{v} \in \boldsymbol{V}$ *and* $q \in L^2(\Omega)$.

The Lagrange multipliers λ_i have the physical meaning of normal stress on the artificial sections (see [3]).

Remark 3.1. Among all the possible Neumann boundary conditions fitting the desired flow rate, the augmented formulation prescribes the one which is parallel to the normal direction and which is constant. Therefore, for the effectiveness of this strategy, it is crucial that the computational domain is cut such that the outward normal is parallel to the axial axis and far from branches.

We point out that Problems 4 share the good property, in view of the numerical simulations, of requiring the discretization of a "standard" space $\boldsymbol{V}$.

We have the following result (see [13]):

Proposition 3.1. *For sufficiently smooth data* Q_i *with* $\sum_i |Q_i|$ *and* $\|\boldsymbol{u}_0\|_{\boldsymbol{V}}$ *small enough, Problem 4 is locally well-posed, i.e. there exists a time* $T^* > 0$ *such that a solution* $(\boldsymbol{u}, p, \{\lambda_i\}_{i=1,\ldots,m})$ *exists in* $[0, T^*]$.

DOI: 10.1685/2010CAIM475

The proof of the previous result is based on proving the following *inf-sup* condition:

(10)
$$\exists \beta > 0 : \forall \boldsymbol{\mu} \in \mathbb{R}^m, \exists \boldsymbol{v} \in \boldsymbol{V} : b(\boldsymbol{\mu}, \boldsymbol{v}) = \Big| \sum_{j=1}^{m} \mu_j \int_{\Gamma_j} \boldsymbol{v} \cdot \boldsymbol{n} d\gamma \Big| \geq \beta \|\boldsymbol{\mu}\| \|\boldsymbol{v}\|_{\boldsymbol{V}}$$

Moreover, let us set $m = 1$ and $Q_1 = 0$. Then, we have the following

Proposition 3.2. *The Lagrange multiplier λ satisfies the following a priori estimate*

$$|\lambda_1(t)| \leq \frac{1}{\beta} \Big(C_P \|\boldsymbol{f}\| + C_P \Big\| \frac{\partial \boldsymbol{u}}{\partial t} \Big\| + \mu \|\boldsymbol{u}\|_{\boldsymbol{V}} + C_P \|\boldsymbol{\beta}\|_{\boldsymbol{L}^\infty(\Omega)} \|\boldsymbol{u}\|_{\boldsymbol{V}} \Big).$$

Proof. Let us set $\boldsymbol{v} = \boldsymbol{u}$ in the momentum equation and let us integrate in time. Exploiting that $\int_{\Gamma_1} \boldsymbol{u} \cdot \boldsymbol{n} \, d\gamma = 0$, we obtain the classical regularity results (see [11]):

(11)
$$\boldsymbol{u} \in L^2(0, T^*; \boldsymbol{H}^2(\Omega)), \qquad \boldsymbol{u}' \in L^2(0, T^*; \boldsymbol{L}^2(\Omega))$$

From the *inf-sup* condition (10) we obtain (considering the free-divergence subspace):

$$|\lambda_1(t)| \leq \frac{1}{\beta} \sup_{\boldsymbol{v} \in \boldsymbol{V}^*} \frac{\lambda_1 \int_{\Gamma_1} \boldsymbol{v} \cdot \boldsymbol{n} \, d\gamma}{\|\boldsymbol{v}\|_{\boldsymbol{V}}} =$$

$$\frac{1}{\beta} \sup_{\boldsymbol{v} \in \boldsymbol{V}^*} \frac{(\boldsymbol{f}, \boldsymbol{v}) - \Big(\frac{\partial \boldsymbol{u}}{\partial t}, \boldsymbol{v} \Big) - \mu(\nabla \boldsymbol{u}, \nabla \boldsymbol{v}) - ((\boldsymbol{\beta} \cdot \nabla)\boldsymbol{u}, \boldsymbol{v})}{\|\boldsymbol{v}\|_{\boldsymbol{V}}} \leq$$

$$\leq \frac{1}{\beta} \sup_{\boldsymbol{v} \in \boldsymbol{V}^*} \frac{\|\boldsymbol{f}\| \, \|\boldsymbol{v}\| + \Big\| \frac{\partial \boldsymbol{u}}{\partial t} \Big\| \, \|\boldsymbol{v}\| + \mu \|\boldsymbol{u}\|_{\boldsymbol{V}} \|\boldsymbol{v}\|_{\boldsymbol{V}} + \|\boldsymbol{\beta}\|_{\boldsymbol{L}^\infty(\Omega)} \|\boldsymbol{u}\|_{\boldsymbol{V}} \|\boldsymbol{v}\|}{\|\boldsymbol{v}\|_{\boldsymbol{V}}}$$

where with $\|\cdot\|$ we indicate the $L^2(\Omega)$ norm and where $\|\boldsymbol{w}\|_{\boldsymbol{V}} = \|\nabla \boldsymbol{w}\|$. Exploiting the Poincaré inequality (with constant C_P) and from the regolarity results (11), we obtain that all the terms at the right hand side are in $L^2(0, T^*)$ and therefore the thesis follows and we conclude that $\lambda_1 \in L^2(0, T^*)$. □

The extension of the previous results to the case $m > 1$ and $Q_j \neq 0$ is straightforward.

4. Numerical algorithms

We want now to investigate some modular numerical methods for the approximation of the augmented problems. In the sequel, we refer to a finite element discretization of the Oseen equations, featuring the *inf-sup* compatible elements (see [1,9]). In particular, let us denote $\boldsymbol{V}_h$ and Q_h the subspaces of $\boldsymbol{V}$ and $L^2(\Omega)$ of dimension N_u and N_p and with basis functions denoted by $\boldsymbol{\psi}_j$ and ζ_k, respectively. Moreover, let us denote with Ω_h the numerical computational domain obtained with a partition τ_h of Ω in elements K_j.

Let us introduce a partition of the time interval $[0, T]$ into subintervals. For the sake of simplicity, we refer to a uniform subdivision with size Δt. Among the other methods for the time advancing, we consider a discretization of the time derivatives based on the Backward Difference Formulas (BDF) (see [6]). Setting $t^n = n\Delta t$, for $n = 0, 1, \ldots$, we have the following:

Problem 5. *Given $\boldsymbol{u}_{0,h}$ suitable approximation of the initial guess $\boldsymbol{u}_0$ and posing $\boldsymbol{f}^n = \boldsymbol{f}(t^n, \boldsymbol{x})$, $\boldsymbol{\beta}^n = \boldsymbol{\beta}(t^n, \boldsymbol{x})$ and $Q_j^n = Q_j(t^n)$, $j = 1, \ldots, m$, find $\boldsymbol{u}_h^{n+1}(t) \in \boldsymbol{V}_h$, $p_h^{n+1} \in Q_h$ and $\boldsymbol{\lambda}_h^{n+1} \in \mathbb{R}^m$ such that, for each n:*

$$
\begin{cases}
\dfrac{\alpha}{\Delta t}\Big(\boldsymbol{u}_h^{n+1}, \boldsymbol{v}_h\Big) + a(\boldsymbol{u}_h^{n+1}, \boldsymbol{v}_h) + ((\boldsymbol{\beta}^{n+1} \cdot \nabla)\boldsymbol{u}_h^{n+1}, \boldsymbol{v}_h) + b(p_h^{n+1}, \boldsymbol{v}_h) + \\
\quad + \displaystyle\sum_{j=1}^{m} \lambda_{j,h}^{n+1} \int_{\Gamma_j} \boldsymbol{v}_h \cdot \boldsymbol{n}\, d\gamma = (\boldsymbol{f}^{n+1}, \boldsymbol{v}_h) + \sum_{j=0}^{r \le n} \frac{\tau_j}{\Delta t}\Big(\boldsymbol{u}_h^{n-j}, \boldsymbol{v}_h\Big), \ \boldsymbol{x} \in \Omega_h \\
b(q_h, \boldsymbol{u}_h^{n+1}) = 0, \qquad \boldsymbol{x} \in \Omega_h \\
\boldsymbol{u}_h^0 = \boldsymbol{u}_{0,h}, \qquad \boldsymbol{x} \in \Omega_h \\
\displaystyle\int_{\Gamma_i} \boldsymbol{u}_h^{n+1} \cdot \boldsymbol{n}\, d\gamma = Q_i^{n+1} \quad \forall i = 1, \ldots, m,
\end{cases}
$$

for all $\boldsymbol{v}_h \in \boldsymbol{V}_h$ and $q_h \in Q_h$ and where α and τ_j, $j = 0, \ldots, r$, are the coefficients of the time discretization.

The algebraic form of the augmented discrete problem is therefore given by:

$$
\begin{bmatrix} K & B^t & \Phi^t \\ B & 0 & 0 \\ \Phi & 0 & 0 \end{bmatrix} \begin{bmatrix} \boldsymbol{U}^{n+1} \\ \boldsymbol{P}^{n+1} \\ \boldsymbol{\Lambda}^{n+1} \end{bmatrix} = \begin{bmatrix} \widetilde{\boldsymbol{F}}^{n+1} \\ \boldsymbol{0} \\ \boldsymbol{Q}^{n+1} \end{bmatrix} \tag{12}
$$

where $\boldsymbol{U}^{n+1}$ and $\boldsymbol{P}^{n+1}$ are the vectors of the nodal values of the velocity and of the pressure field respectively and $\boldsymbol{\Lambda}^{n+1}$ is the vector of the approximated Lagrange multipliers at time step $n+1$, $K = K^{n+1} = \dfrac{\alpha}{\Delta t} M + A + C$ sums up the discretization of the time derivative (mass matrix $M = [m_{ij}] =$

DOI: 10.1685/2010CAIM475

$[(\boldsymbol{\psi}_i, \boldsymbol{\psi}_j)]$), of the viscous term (stiffness matrix $A = [a_{ij}] = [a(\boldsymbol{\psi}_i, \boldsymbol{\psi}_j)]$) and of the convective one (matrix $C = C^{n+1} = [c_{ij}] = [((\boldsymbol{\beta}^{n+1} \cdot \nabla)\boldsymbol{\psi}_i, \boldsymbol{\psi}_j)]$. In all these three cases we have $i, j = 1, \ldots, N_u$. Finally, $B = [b_{il}] = [b(\zeta_l, \boldsymbol{\psi}_i)]$, for $l = 1, \ldots, N_p$ and $i = 1, \ldots, N_u$, $\Phi = [\phi_{rj}] = [\int_{\Gamma_r} \boldsymbol{\psi}_j \cdot \boldsymbol{n}\, d\gamma]$, for $r = 1, \ldots, m$ and $j = 1, \ldots, N_u$, and $\widetilde{\boldsymbol{F}}^{n+1} = \boldsymbol{F}^{n+1} + \sum_{j=0}^{r \le n} \frac{\tau_j}{\Delta t} M \boldsymbol{U}^{n-j}$, with $\boldsymbol{F} = [F_i] = (\boldsymbol{f}, \boldsymbol{\psi}_i)$. We have the following result:

Proposition 4.1. *Under the same regularity assumptions of Proposition 3.1, Problem 5 admits a unique solution if*

$$\Delta t < \min_{\{\boldsymbol{w}_h \neq \boldsymbol{0}\}} \frac{\alpha |\boldsymbol{w}_h^t M \boldsymbol{w}_h|}{|\boldsymbol{w}_h^t C \boldsymbol{w}_h|}. \tag{13}$$

Proof. In order to prove the well posedness of Problem 5, it is sufficient to prove that under condition (13), matrix K is positive definite, i.e. that

$$\boldsymbol{w}_h^t K \boldsymbol{w}_h > 0, \quad \forall \boldsymbol{w}_h \neq \boldsymbol{0},$$

Since A is positive definite (see [9]), we require that:

$$\frac{\alpha}{\Delta t} \boldsymbol{w}_h^t M \boldsymbol{w}_h + \boldsymbol{w}_h^t C \boldsymbol{w}_h > 0, \quad \forall \boldsymbol{w}_h \neq \boldsymbol{0}$$

yielding the thesis. □

For the approximation of the augmented Navier-Stokes problem, we consider, if not differently specified, a semi-implicit discretization. In particular, we set $\boldsymbol{\beta}^{n+1} = \boldsymbol{u}_h^n$ in Problem 5 and in (12).

4.1. *Schur complement scheme + GMRes (Scheme I)*

We rewrite (12) in a more compact form:

$$\begin{bmatrix} N & \widetilde{\Phi}^t \\ \widetilde{\Phi} & 0 \end{bmatrix} \begin{bmatrix} \boldsymbol{X}^{n+1} \\ \boldsymbol{\Lambda}^{n+1} \end{bmatrix} = \begin{bmatrix} \boldsymbol{H}^{n+1} \\ \boldsymbol{Q}^{n+1} \end{bmatrix} \tag{14}$$

where $N = \begin{bmatrix} K & B^t \\ B & 0 \end{bmatrix}$. Since the discrete inf-sup condition holds, N is non-singular, so we can reduce system (14) by eliminating $\boldsymbol{X}^{n+1}$ as:

$$\widetilde{\Phi} N^{-1} \widetilde{\Phi}^t \boldsymbol{\Lambda}^{n+1} = \widetilde{\Phi} N^{-1} \boldsymbol{H}^{n+1} - \boldsymbol{Q}^{n+1},$$

where N^{-1} indicates the solution of a Oseen or of a linearized Navier-Stokes problem. Matrix $R = \widetilde{\Phi} N^{-1} \widetilde{\Phi}^t$ is the *Schur complement* associated

to (14). In [3], the previous problem for the Lagrange multipliers has been introduced for the steady Stokes problem and a Coniugate Gradient method has been proposed for its soution. Nevertheless, since N is not symmetric in the general case, we make use of the GMRes method as iterative solver for the computation of $\mathbf{\Lambda}^{n+1}$ (see [13]). We notice that a system in N has to be preliminarily solved for the computation of the initial residual. Then, since GMRes converges in at most m iterations (recall that m is the number of sections where flow rate conditions are prescribed, so it is usually a small number), further m systems in N are solved to compute the residual at each iteration. Finally, once $\mathbf{\Lambda}$ has been computed, a further system in N should be solved for the computation of the velocity and the pressure fields. However, the residual computation in the last GMRes step on the converged solution already entails the solution of the latter system in N, so that the final velocity-pressure computation actually makes use of an algebraic manipulation of vectors. *This means that $m+1$ systems in N at each time step are required for this scheme*. Moreover, to solve a system for N actually corresponds to the solution of a Oseen or of a linearized Navier-Stokes problem with Neumann conditions on the sections where the flow rate is prescribed. This can be pursued, for example, by means of a given (generic) solver and makes Scheme I modular.

4.2. *Inexact splitting (Scheme II)*

The drawback of Scheme I is that the computation of the solution is obtained by using an iterative procedure: the iterative solver (GMRes) for the resolution of the linear system in $\mathbf{\Lambda}$. Therefore the computational costs of this strategy could be quite expensive in practical applications. In this section we propose an approximate (inexact) algorithm for the solution of the augmented problem, introduced in [14]. Since this approach does not require an iterative approach, it yields a significant reduction of the computational costs. This strategy is based on an exact continuous splitting of the augmented formulation. In the sequel, we firstly introduce the exact splitting. Then, we propose its approximation that leads to Scheme II. We refer to the augmented Oseen problem (9). More precisely, consider the following scheme:

1. *Solve for $i = 1, \dots, m$ the following steady Neumann problems in the unknowns $\boldsymbol{w}_i$ and π_i*:

$$\begin{cases} a(\boldsymbol{w}_i, \boldsymbol{v}) + b(\pi_i, \boldsymbol{v}) = -\displaystyle\int_{\Gamma_i} \boldsymbol{v} \cdot \boldsymbol{n} d\gamma \\ b(q, \boldsymbol{w}_i) = 0, \end{cases} \tag{15}$$

DOI: 10.1685/2010CAIM475

$\forall \boldsymbol{v} \in \boldsymbol{V}, \forall q \in L^2(\Omega)$.

2. *Solve the following unsteady Neumann homogeneous problem in the unknowns* $\boldsymbol{s}$ *and* ξ:

$$\begin{cases} \left(\dfrac{\partial \boldsymbol{s}}{\partial t}, \boldsymbol{v}\right) + a(\boldsymbol{s}, \boldsymbol{v}) + ((\boldsymbol{\beta} \cdot \nabla)\boldsymbol{s}, \boldsymbol{v}) + b(\xi, \boldsymbol{v}) = (\boldsymbol{f}, \boldsymbol{v}) \\ b(q, \boldsymbol{s}) = 0, \end{cases} \tag{16}$$

$\forall \boldsymbol{v} \in \boldsymbol{V}, \forall q \in L^2(\Omega)$, with the initial condition $\boldsymbol{s}|_{t=0} = \boldsymbol{u}_0$.

3. *Solve a linear system.* Let B be the matrix given by

$$B_{ij} = \int_{\Gamma_i} \boldsymbol{w}_j \cdot \boldsymbol{n} d\gamma,$$

and $\boldsymbol{S}$ the vector with elements

$$S_i = \int_{\Gamma_i} \boldsymbol{s} \cdot \boldsymbol{n} d\gamma.$$

Let us denote with $\boldsymbol{Q}$ the vector with components Q_i $(i = 1, \ldots, m)$. We find therefore the vector $\boldsymbol{\eta}(t)$ by solving

$$\mathrm{B}\boldsymbol{\eta} = \boldsymbol{Q} - \boldsymbol{S}.$$

4. *Solve the following unsteady augmented homogeneous problem.* Find $\boldsymbol{e} \in L^2(0, T, \boldsymbol{V}) \cap L^\infty(0, T, \boldsymbol{L}^2(\Omega))$, $\varepsilon \in L^2(0, T, L^2(\Omega))$ and $\boldsymbol{\nu} \in (L^2(0, T))^m$ such that for all $\boldsymbol{v} \in \boldsymbol{V}$, $q \in L^2(\Omega)$:

$$\begin{cases} \left(\dfrac{\partial \boldsymbol{e}}{\partial t}, \boldsymbol{v}\right) + a(\boldsymbol{e}, \boldsymbol{v}) + ((\boldsymbol{\beta} \cdot \nabla)\boldsymbol{e}, \boldsymbol{v}) + b(\varepsilon, \boldsymbol{v}) + \displaystyle\sum_{i=1}^{m} \nu_i \int_{\Gamma_i} \boldsymbol{v} \cdot \boldsymbol{n} d\gamma = \\ \qquad = -\displaystyle\sum_{j=1}^{m} \frac{d\eta_j}{dt}(\boldsymbol{w}_j, \boldsymbol{v}) - \sum_{j=1}^{m} \eta_j ((\boldsymbol{\beta} \cdot \nabla)\boldsymbol{w}_j, \boldsymbol{v}) \\ b(q, \boldsymbol{e}) = 0 \\ \displaystyle\int_{\Gamma_i} \boldsymbol{e} \cdot \boldsymbol{n} d\gamma = 0 \qquad i = 1, 2, \ldots m \end{cases}, \tag{17}$$

with the initial condition: $\boldsymbol{e}|_{t=0} = \boldsymbol{0}$.

It is possible to verify by linear combination that solution of problem (9) can be written as:

$$\begin{cases} \boldsymbol{u} = \boldsymbol{s} + \boldsymbol{e} + \sum_{j=1}^{m} \eta_j \boldsymbol{w}_j, \\ p = \xi + \varepsilon + \sum_{j=1}^{m} \eta_j \pi_j, \\ \lambda_i = \nu_i + \eta_i \quad \forall i = 1, 2, \dots m. \end{cases}$$

It is worth noting that all the subproblems are well posed under suitable assumptions (see [14]). The steady problems are obviously to be solved once at all at the beginning of computations.

Remark 1. If $\boldsymbol{f} = \boldsymbol{0}$ and $\boldsymbol{u}_0 = \boldsymbol{0}$ problem (16) admits the trivial solution $\boldsymbol{s} = \boldsymbol{0}$ and $\xi = 0$. By exploiting this circumstance, in this case numerical solution of (16) can be dropped.

In the previous splitting, we compute separately the contributions to the solution given by the forcing term and the flow rates. The latter still requires the solution of an augmented (homogeneous) problem, and it is expensive to solve. We therefore approximate problem (17) with the following one. Let us set $\hat{\Gamma} \equiv \Gamma_w \cup \Gamma_1 \cup \ldots \cup \Gamma_m \equiv \partial\Omega \setminus \Gamma_0$.

Problem 6. *Find* $\hat{\boldsymbol{e}} \in L^2(0, T, \boldsymbol{H}^1_{\hat{\Gamma}}(\Omega)) \cap L^\infty(0, T, \boldsymbol{L}^2(\Omega))$ *and* $\hat{\varepsilon} \in L^2(0, T, L^2(\Omega))$ *such that for all* $\boldsymbol{v} \in \boldsymbol{H}^1_{\hat{\Gamma}}(\Omega)$, $q \in L^2(\Omega)$*:*

$$\begin{cases} \left(\dfrac{\partial \hat{\boldsymbol{e}}}{\partial t}, \boldsymbol{v}\right) + a\left(\hat{\boldsymbol{e}}, \boldsymbol{v}\right) + \left(\left(\boldsymbol{\beta} \cdot \nabla\right) \hat{\boldsymbol{e}}, \boldsymbol{v}\right) + b\left(\hat{\varepsilon}, \boldsymbol{v}\right) = \\ \qquad\qquad = -\sum_{j=1}^{m} \dfrac{d\eta_j}{dt} \left(\boldsymbol{w}_j, \boldsymbol{v}\right) - \sum_{j=1}^{m} \eta_j \left(\left(\boldsymbol{\beta} \cdot \nabla\right) \boldsymbol{w}_j, \boldsymbol{v}\right) \\ b\left(q, \hat{\boldsymbol{e}}\right) = 0 \end{cases} \tag{18}$$

with the initial condition: $\hat{\boldsymbol{e}}|_{t=0} = \boldsymbol{0}$.

This is a standard Oseen problem with homogeneous Dirichlet conditions on $\hat{\Gamma}$.

Remark 2. Observe that in the steady Stokes case, namely for $\dfrac{d\eta_j}{dt} = 0$ for each $j = 1, 2, \ldots, m$, problem (17) and (18) both have the unique solution $\boldsymbol{e} = \hat{\boldsymbol{e}} = \boldsymbol{0}$. In this case, therefore, Scheme II yields the exact solution.

DOI: 10.1685/2010CAIM475

We observe that Scheme II does not make use iterative strategies anymore and that the computation is obtained by solving just 2 (1 if $\boldsymbol{f} = \boldsymbol{u}_0 = \mathbf{0}$) Oseen problems. Again, we have obtained a modular algorithm.

The price to pay is the following: the null flux problem is still an augmented problem and therefore, in solving it approximatively, we introduce an error in a small neighborhood of the artificial sections where the flow rate is prescribed. From the practical viewpoint, this means that correct numerical results can be obtained in the region of interest by working in a slightly extended computational domain. Even when working with a larger domain, in fact, the computational times of the present method are significantly reduced with respect to the "exact" Lagrange multiplier approaches (Scheme I), yielding comparable numerical results in the region of interest (see Section 5).

Observe that since the error in Scheme II has been introduced by forcing a null velocity profile (Dirichlet condition) in (18) instead of a null flow rate, as a matter of fact, we are prescribing a "wrong" velocity profile. Therefore, we can refer to the error analysis proposed in [14], where it has been proved that the error introduced in prescribing an arbitrary velocity profile increases for an increasing Reynolds number. Then, as the numerical results in [14] highlight, the errors made with this strategy are less than the ones done by imposing directly a parabolic or a flat profile fitting the desired flow rate (as in the *practical approach*). Indeed, in problem (18) we are imposing a null Dirichlet boundary condition, i.e. we are considering a problem with small Reynolds number near the boundary. Therefore, the error is smaller than the one made imposing directly a non-null velocity profile (as in the *practical approach*), where *Re* could be very big.

The present proposal could therefore be considered as an intermediate and reliable approach between the engineering one (*practical approach*), requiring a relevant expansion of the domain for loosing the effects of the arbitrary velocity profile selection, and the exact one based on the augmented reformulation.

Remark 3. As an alternative, in order to save computational times, it would be possible to treat system (12) monolithically, by studying other splitting schemes which group the Lagrange multipliers with the velocity or the pressure unknowns. However, these schemes would lead to non-classical Oseen or Stokes problem, and therefore they would be non-modular. For this reason, we do not consider them in this work.

5. Numerical results

Scheme I and Scheme II have been used to simulate a carotid domain starting from real data of a patient (see Figure 7). We observe that the geometry was cut such that the normal is parallel to tha axial axis, so that the Augmented formulation should be effective (see Remark 3.1). The viscosity has been setted equal to $0.035\, g/(cm\, s)$. We have used the 3d Finite Element Library *LifeV*, developed at *M.O.X - Dipartimento di Matematica - Politecnico di Milano*, at *CMCS - EPFL of Lausanne* and at *INRIA - Paris* and written in *C++*. We have imposed the physiological flow rates depicted in Figure 6 at the inlet and at the internal outlet of the domain,

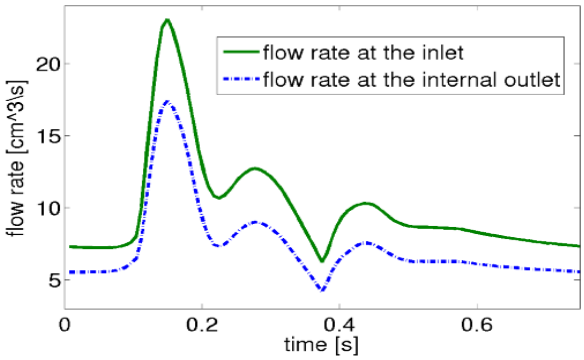

Fig. 6. Prescribed physiological flow rates.

which corresponds to the *internal carotid* (that is the outlet at the right in Figure 7). We consider the Navier-Stokes equations. For the non linear term, we have used a *semi-implicit* treatment, where the convective term $\boldsymbol{u}^{n+1}$ has been approximated by the velocity field at the previous time step $\boldsymbol{u}^n$. The time discretization parameter is $\Delta t = 0.008\, s$, which leads to stable solutions, so that we can argue that condition (13) is satisfied.

Figures 7 shows the velocity fields obtained with Scheme I, with Scheme II and imposing a parabolic velocity profile at the inlet and a flat velocity profile at the internal outlet (both fitting the prescribed flow rates), respectively. It is evident that the error made with Scheme II is confined near the boundary and that the enlarged zone requested by the latter is smaller than the one needed by the *practical approach*. Moreover, the latter approach seems to give a numerical solution that does not agree very well with the one obtained using Scheme I. In particular, we point out big differences also far from the artificial sections, in particular at the bifurcation near the wall.

It is worth pointing out the influence of the geometry on the solution

DOI: 10.1685/2010CAIM475

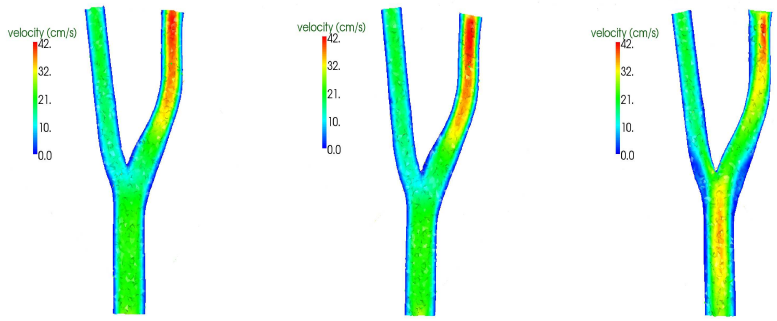

Fig. 7. Computations in 3D: carotid solution. Velocity field obtained with Scheme I (left), Scheme II (middle) and with the *practical approach* (right). $t = 0.225\,s$, $\Delta t = 0.0075\,s$

of the Navier-Stokes problem. Figure 8 shows the velocity field at the inlet of the carotid bifurcation computed by using Scheme I (left) and imposed as parabolic (right). Let us notice the asymmetry of the velocity profile recovered without prescribing it using Scheme I. We think that this solution is more realistic that the one obtained with the practical approach, which cannot be asymmetric. Therefore, for a non-cylindrical domain, the prescription of a parabolic velocity profile or even of the Womersley solution as Dirichlet boundary condition leads anyway to an error due to the effect of the geometry.

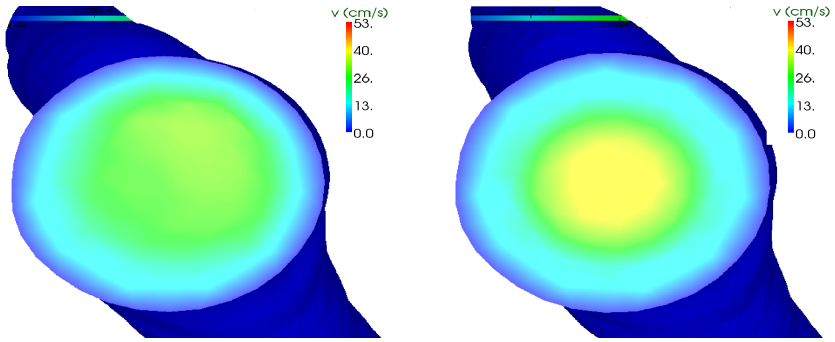

Fig. 8. Computations in 3D: carotid solution. Velocity field at the inlet prescribed with Scheme I (left) with the *practical approach* (right). $t = 0.195\,s$, $\Delta t = 0.0075\,s$.

6. Conclusions

In this paper we have reviewed two modular algorithms for the solution of the flow rate boundary value problem. We have shown the differences of the solutions obtained with these schemes and with the classical practical

approach, in a realistic domain, namely the human carotid. The application of such techniques for clinical purposes seems to be very promising, as already shown in the first two studies in this direction, namely for the estimation of the flow rate measure (see [8]) and in the study of the fluid-dynamics in the bicuspid valve's configuration (see [15]).

Acknowledgments

The author would like to thank the INDAM-SIMAI for the prize for the Ph.D. theses in applied mathematics and for the invitation to submit a paper on this journal.

REFERENCES

1. F. Brezzi. On the existence, uniqueness and approximation of saddle point problems arising from lagrange multipliers. *RAIRO Anal. Numer.*, 8:129–151, 1974.
2. L. Formaggia, J.-F. Gerbeau, F. Nobile, and A. Quarteroni. On the coupling of 3D an 1D Navier-Stokes equations for flow problems in compliant vessels. *Computer Methods in Applied Mechanics and Engineering*, 191(6-7):561–582, 2001.
3. L. Formaggia, J.-F. Gerbeau, F. Nobile, and A. Quarteroni. Numerical treatment of defective boundary conditions for the Navier-Stokes equation. *SIAM Journal on Numerical Analysis*, 40(1):376–401, 2002.
4. J.G. Heywood, R. Rannacher, and S. Turek. Artificial boundaries and flux and pressure conditions for the incompressible Navier-Stokes equations. *International Journal for Numerical Methods in Fluids*, 22:325–352, 1996.
5. O. Ladyzhenskaya. *The mathematical theory of viscous incompressible flow*. Gordon and Breach, New York, 1969.
6. R.J. LeVeque. *Finite Difference Methods for Differential Equations*. On line Lecture Notes, 2005.
7. L. Morris, P. Delassus, P. Grace, F. Wallis, M. Walsh, and T. McGloughlin. Effects of flat, parabolic and realistic steady flow inlet profiles on idealised and realistic stent graft fits through abdominal aortic aneurysms (aaa). *Med. Eng. Phys.*, 28:19–26, 2006.
8. R. Ponzini, C. Vergara, A. Redaelli, and A. Veneziani. Reliable cfd-based estimation of flow rate in haemodynamics measures. *Ultrasound in Medicine and Biology*, 32(10):1545–1555, 2006.
9. A. Quarteroni and A. Valli. *Numerical approximation of partial differential equations*. Springer, 1994.
10. A. Redaelli, F. Boschetti, and F. Inzoli. The assignement of velocity

DOI: 10.1685/2010CAIM475

profiles in finite element simulations of pulsatile flow in arteries. *Comput. Biol. Med.*, 27(3):233–247, 1997.

11. R. Temam. *Navier-Stokes equations and nonlinear functional analysis*. SIAM, Philadelphia, 1995.
12. A. Veneziani. *Mathematical and Numerical Modeling of Blood Flow Problems*. PhD thesis, University of Milan, 1998.
13. A. Veneziani and C. Vergara. Flow rate defective boundary conditions in haemodinamics simulations. *International Journal for Numerical Methods in Fluids*, 47:803–816, 2005.
14. A. Veneziani and C. Vergara. An approximate method for solving incompressible Navier-Stokes problems with flow rate conditions. *Computer Methods in Applied Mechanics and Engineering*, 196(9-12):1685–1700, 2007.
15. F. Viscardi, C. Vergara, L. Antiga, S. Merelli, A. Veneziani, G. Puppini, G. Faggian, A. Mazzucco, and G.B. Luciani. Comparative finite-element model analysis of ascending aortic flow in bicuspid and tricuspid aortic valve. *Artificial Organs*, in press.
16. S. Whitaker. *Introduction to Fluid Mechanics*. R.E. Krieger, Malabar, FL, 1984.
17. J. R. Womersley. Oscillatory motion of a viscous liquid in a thin-walled elastic tube: I. the linear approximation for long waves. *Philosophical magazine*, 46:199–221, 1955.